nature COMMUNICATIONS

ARTICLE

Received 31 Dec 2013 | Accepted 26 Mar 2014 | Published 24 Apr 2014

DOI: 10.1038/ncomms4725

Fractal free energy landscapes in structural glasses

Patrick Charbonneau[1,2,3], Jorge Kurchan[4], Giorgio Parisi[5,6], Pierfrancesco Urbani[7] & Francesco Zamponi[3]

Glasses are amorphous solids whose constituent particles are caged by their neighbours and thus cannot flow. This sluggishness is often ascribed to the free energy landscape containing multiple minima (basins) separated by high barriers. Here we show, using theory and numerical simulation, that the landscape is much rougher than is classically assumed. Deep in the glass, it undergoes a 'roughness transition' to fractal basins, which brings about isostaticity and marginal stability on approaching jamming. Critical exponents for the basin width, the weak force distribution and the spatial spread of quasi-contacts near jamming can be analytically determined. Their value is found to be compatible with numerical observations. This advance incorporates the jamming transition of granular materials into the framework of glass theory. Because temperature and pressure control what features of the landscape are experienced, glass mechanics and transport are expected to reflect the features of the topology we discuss here.

[1] Department of Chemistry, Duke University, Durham, North Carolina 27708, USA. [2] Department of Physics, Duke University, Durham, North Carolina 27708, USA. [3] LPT, École Normale Supérieure, UMR 8549 CNRS, 24 Rue Lhomond, 75005 Paris, France. [4] LPS, École Normale Supérieure, UMR 8550 CNRS, 24 Rue Lhomond, 75005 Paris, France. [5] Dipartimento di Fisica, Sapienza Università di Roma, P.le A. Moro 2, I-00185 Roma, Italy. [6] INFN, Sezione di Roma I, IPFC—CNR, P.le A. Moro 2, I-00185 Roma, Italy. [7] IPhT, CEA/DSM-CNRS/URA 2306, CEA Saclay, F-91191 Gif-sur-Yvette Cedex, France. Correspondence and requests for materials should be addressed to P.U. (email: pierfrancesco.urbani@cea.fr).

Understanding the dynamics of glasses is one of the oldest and most challenging problems in the theory of matter. The classical thermodynamic picture interprets the slow relaxation of glasses in terms of a free energy landscape with fairly simple structural features (Fig. 1): each minimum is a stable amorphous glass state, high frequency relaxations correspond to vibrational excitations of the state and slow relaxations correspond to jumps between different states[1–3]. Yet experimental and numerical observations suggest that this simple landscape description—with essentially only one type of barrier—is insufficient to capture the complexity of glassy dynamics. Low-temperature glasses exhibit an intermediate slow (Johari-Goldstein) relaxation whose timescale is indeed difficult to interpret as one corresponding to jumps between widely different states[4]. It has thus been proposed that the landscape features narrow sub-basins, separated by small barriers, that aggregate into wider metabasins, separated by large barriers (Fig. 1). Johari-Goldstein relaxation processes would then connect sub-basins within a same metabasin[4,5]. Direct numerical investigations have confirmed the metabasin organization and thereby improved the phenomenological description of transport[6,7]. Deep within the glass phase, the out-of-equilibrium dynamics is also unable to properly sample the distribution of barriers associated with the complex sub-basin structure, which could explain why describing it with a single fictive temperature is not possible[8,9].

A disordered ensemble of (nearly) hard spheres, that is, spherical particles that cannot overlap, is often taken as a simple model for glasses, both in theoretical and experimental studies. The behaviour of static assemblies of macroscopic spheres[10], colloidal suspensions[11–13] and dynamically agitated ensembles of grains[14] is indeed akin to that of thermal glasses. Like thermal glasses, hard spheres can also be theoretically described in terms of a complex free energy landscape dominated by entropic effects[15]; the same analysis tools can be used for both systems[16], underlying the similarity of their dynamical behaviour[17] and of their phase diagram in terms of pressure and density[18]. In addition, when hard sphere interactions are considered, a new kind of geometric phase transition appears, the jamming transition[19–21], that can be characterized in two equivalent ways. From a thermodynamic point of view, compressing a hard sphere glass to infinite pressure results in an amorphous jammed packing in which particles are completely arrested and mechanically equilibrated[18]. From a rheological point of view, hard sphere glass rigidity is entropic before reaching the jamming transition, and (relaxing the harshness of the hard sphere repulsion) mechanical beyond jamming, as in low-temperature molecular glasses[22]. On approaching jamming, hard sphere glasses are marginally stable[23–25]: they have very soft vibrational modes and excitations that extend over a wide range of timescales[19,25] and can be characterized in terms of critical scalings similar to ordinary phase transitions, see refs 20,21 for reviews. The critical properties of the jamming transition hence provide additional insights into the structure of the landscape. Yet neither the marginality of the basins nor the smallness of the barriers associated with the soft modes fit in the simple landscape picture[18], which is hence unable to explain the critical properties of the jamming transition.

In the late eighties, Kirkpatrick, Thirumalai and Wolynes proposed that mean-field disordered models contain the essential features of glassy landscapes[26–28]. These models fall in two broad universality classes: the so-called Random First Order (the simple picture of a stable glass, with featureless basins and large barriers)[26,27] and another class where one large state is broken up in a fractal hierarchy of basins within basins, discovered by one of us in the Sherrington-Kirkpatrick (SK) model[29,30]. The first class yields, close to the glass transition, a two-step dynamical relaxation[31] in the same universality class as the mode-coupling theory[17,32]. It was thus taken to represent (fragile) structural glasses, at least close to the glass transition—hence the name Random First Order Transition (RFOT) associated with this

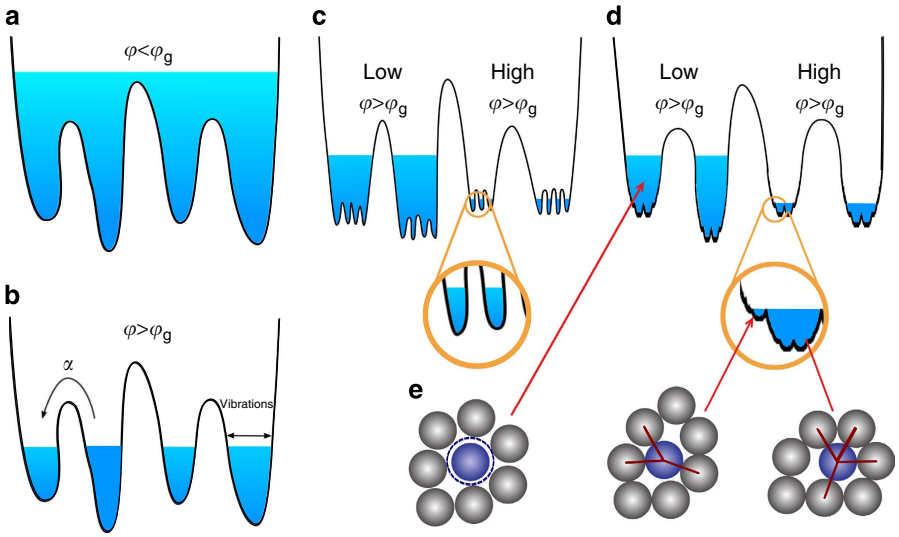

Figure 1 | Free energy landscape with simple basins, metabasins and fractal basins. Schematic depictions of (**a**) the liquid state at packing fractions φ that are smaller than the glass transition φ_g, and of free energy basins for different landscape scenarios: (**b**) simple stable basins, (**c**) metabasins of sub-basins (**d**) and metabasins of marginal basins. The simple landscape description is akin to boating on a system of lakes separated by high mountains. In the liquid, all of space can be explored. At lower water levels, each basin is a different glass. The free energy barriers hinder passing from one glass to another (the so-called α-relaxation); the basin width allows for vibrational relaxation. Both in **c** and **d**, the water level further determines what features of the landscape are experienced. Deep into the glass, the landscape roughness results in intra-state barriers that are associated with secondary relaxations. In **d**, at very low water levels (right)—deep into the fractal glass—lakes transform into a complex wetland with a hierarchy of small ponds. (**e**) The very bottom of each of these ponds corresponds to a given realization of the force network (red lines), but the identification of the force contacts remains undetermined before the fractal regime is reached (dashed line).

proposal. Gardner, however, introduced a twist to this classification[33]. She found that, when continued deep in the glass phase, RFOT systems generically reach another phase transition. At this transition, each individual amorphous state (basin) becomes a metabasin by breaking into a full fractal hierarchy of sub-basins akin to that of the SK model, while retaining its identity as a metabasin. Surprisingly, despite an early comment to the effect that this 'fractal phase' might be related to secondary relaxations in real glasses[26], it has since remained somewhat of an intellectual curiosity.

Although the RFOT scenario was initially proposed as an analogy, today we know it to be exact for particles in the limit of large spatial dimensions d (refs 34–36). Solving a problem through an expansion around the limit $d\to\infty$ is an established strategy in quantum mechanics, atomic physics and statistical mechanics when there are no small parameters[37,38], and the glass problem is no exception. The question whether a given feature is captured by RFOT then becomes whether that same feature extrapolates continuously from $d=3$ to $d\to\infty$, a fact that may be checked with numerical simulations. It is numerically found that the main features of the bottom of the basins, which are related to jamming, are extremely stable with varying dimension[39–41]; note by contrast that the behaviour of high barriers, which are connected to the relaxation around the glass transition, remains the object of lively debates[2,42,43].

The main object of this paper is to report that the exact hard sphere solution in the limit $d\to\infty$ predicts the existence of a Gardner transition to a fractal phase in the glass regime, and that taking this transition into account is crucial to understanding the physics of jamming (Fig. 1). It affects the out-of-equilibrium dynamics deep in the glass phase[9,44–46], incorporating (at least partially) secondary relaxations, a point that we here only briefly touch upon. Sub-basins and barriers of a wide variety of sizes also bring along marginality and soft modes, features that were absent in the original RFOT scenario. Their inclusion allows us to make contact with and incorporate the features of jamming theory associated with marginality and isostaticity[23–25]. More specifically, we show that (i) the marginal and fractal phase deep inside hard sphere glasses fully contains the jamming transition; (ii) taking this result into account, one can make analytic predictions for the critical exponents of the jamming transition that are fully compatible with observations; and (iii) one can compute the probability distribution of the forces in jammed packings, which displays an analogue of the Coulomb gap[47], resulting in a power-law scaling of the distribution of small forces[40,48]. Because the critical properties of jamming are independent of spatial dimension[39–41], the results obtained in $d\to\infty$ immediately translate to experimental systems in $d=2$, 3 and hence provide a first unambiguous application of the fractal phase in finite dimension.

Results

Phase diagram. Using an approach similar to that used for solving the SK model, the exact $d\to\infty$ solution for d-dimensional identical hard spheres of unit diameter can be formulated in terms of a caging order parameter $\Delta(y)$ (refs 29,30). This functional order parameter, which encodes the width Δ of metabasins on a (properly defined) scale y, is obtained by numerically solving a set of integro-differential equations (Supplementary Note 1) and then used to calculate the theoretical liquid–glass phase diagram (Fig. 2). The theory predicts that a compressed liquid falls out of equilibrium and becomes a glass at a pressure that depends on the compression rate. Once in a glass state, further compression results in a quick increase of the system pressure p, and on jamming $p\to\infty$ (ref. 18). The final

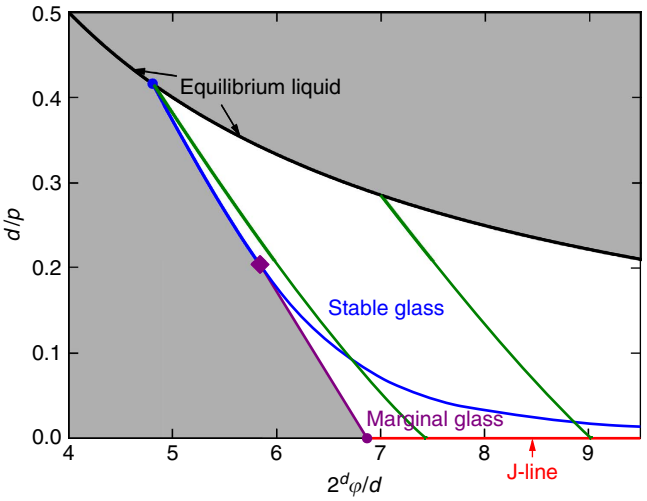

Figure 2 | Phase diagram of infinite-dimensional amorphous hard spheres. Pressure p—packing fraction φ phase diagram for $d\to\infty$ hard spheres. The white region indicates the regime where the (meta)basin structure is present, either as a simple stable glass or as a marginal fractal glass. The left-most boundary of the glass region is the threshold line. The 'J-line' of jammed packings is found along $p=\infty$, which always falls within the marginal phase. Although solving the mean-field out-of-equilibrium dynamics of hard spheres remains an open problem, an adiabatically slow compression should leave the equilibrium liquid line and eventually reach the J-line, while remaining within the white region. The green lines are two examples of an adiabatic following of a glass state[18].

jamming density depends on compression speed, hence defining a J-line of jammed states[18]. Two examples of glass compression obtained using an approximate state following are reported in Fig. 2 (ref. 49).

Independently of compression rate, the glass basin in which the system is initially trapped undergoes a Gardner transition[33], at a line computed in ref. 36. Our key result is that, at pressures above this line, basins transform into metabasins that contain a collection of marginally stable glasses, a phenomenon that is described by a non-trivial caging order parameter $\Delta(y)$ as in the SK model[29]. Finding the solution that describes the marginal phase allows us to delimit the marginal phase boundary (Supplementary Note 1) to within the Gardner transition line of ref. 36, the J-line and the 'threshold' line determined following the prescription of ref. 46. The fact that within this region at least one eigenvalue of the stability matrix in the free energy space vanishes confirms that this phase is indeed marginally stable (Supplementary Note 1)[50]. We also find that, while the radius of the innermost fractal basins shrinks to zero as a power-law $\Delta_{\rm EA}\sim p^{-\kappa}$ (see below), the radius of the largest metabasins remains of order one. Close to jamming, the total entropy of a group of metabasins of width Δ grows as $\Delta^{1/\kappa}$, hence the basins have a phase space structure whose fractal dimension is $2/\kappa$ (see Supplementary Note 1 for a more detailed discussion). The marginal phase is thus also fractal.

The existence of the marginal phase can be qualitatively tested by molecular dynamic (MD) numerical simulations in finite d (Supplementary Note 2) by considering the outcome of a slow compression from the liquid up to jamming[40,51]. Jammed systems are isostatic, and thus particles have an average of $2d$ force-bearing neighbours[19,25,40,52–54], which is much smaller than the $\mathcal{O}(e^d)$ neighbours that isotropically cage a particle in an equilibrated dense liquid. Because the identity of the force-bearing neighbours at jamming uniquely characterizes the state, their emergence sensitively depends on the landscape

structure (Fig. 1). In the simple basin scenario, force-bearing neighbours at jamming should be fully determined immediately on leaving the equilibrium liquid; in the meta/sub-basin scenario, that determination should only occur once sufficiently deep in the glass for transitions between sub-basins to be fully suppressed; in a fractal phase, by contrast, the contacts should be gradually determined as jamming is approached. To test this scenario, we consider a glass configuration at pressure $p_{\rm init}$. Starting from this configuration, we perform several independent compressions up to $p_{\rm f}=10^{10}$ and for each compressed configuration we measure the force network. We obtain a set of contact variables $f_{ij}^{(a)}$, which are set to unity if particles i and j form a force-bearing contact in configuration a and to zero otherwise. The average of $\langle f_{ij}^{(a)} f_{ij}^{(b)}\rangle$ over pairs ab of compressed configurations and over contacts ij provides a measure of similarity between the force networks. The fact that this quantity increases smoothly on increasing $p_{\rm init}$ indicates that the force network is only partially encoded in the initial configuration, in support of the fractal landscape scenario (Fig. 3a and Supplementary Note 2).

Criticality of the jamming transition. The equations that describe the marginal phase are formulated in terms of the caging order parameter $\Delta(y)$ and the pair correlation function $g(r)$, which also encodes the probability distribution of forces in the packing. On approaching the J-line, that is, as a hard sphere glass approaches $p\to\infty$, these equations develop a scaling regime (Fig. 3d) that is characterized by three main critical exponents: θ for the weak forces, α for the quasi-contacts and κ for Δ itself. A (non-trivial) generalization of the approach developed for the SK model[55] allows us to obtain theoretical values for these exponents (Supplementary Note 1). Interestingly, the condition that fixes their value is precisely equivalent to the marginal stability condition. The theory therefore predicts that the criticality of the jamming transition directly follows from its location inside the marginal phase.

A striking signature of marginality is the scaling of the innermost basin width captured by the Edwards-Anderson cage size $\Delta_{\rm EA}\sim p^{-\kappa}$. Although $\kappa=3/2$ was proposed in earlier studies[23,25,56], the theory predicts a slightly smaller $\kappa=1.41574$ that is in remarkable agreement with our numerical results (Fig. 3c). Because single-particle caging by immediate neighbours (a simple Einstein model for glasses) would give $\kappa=2$ (ref. 56), $\kappa<2$ implies that fluctuations near jamming are divergently larger than for independent vibrations, in support of their cooperative nature[25,56]. Note that if one ignores the fractal phase, an explicit computation erroneously gives $\kappa=1$ (ref. 36). Also, note that the exponent κ controls the fractal dimension of the basins, as discussed above.

The pair correlation function $g(r)$ bears a signature of the criticality at the jamming transition. The theory predicts, consistently with the analysis of ref. 57, that when $p\to\infty$, $g(r)$ develops an isostatic contact peak characterized by a scaling function $\mathcal{F}(\lambda)\equiv g(r)/g(1)$ for $\lambda=(r-1)p$ (Fig. 4 and Supplementary Note 1). It also predicts that the scaling function of the contact peak decays as $\mathcal{F}(\lambda)\sim\lambda^{-2-\theta}$ at large λ. The distribution $P(f)$ of inter-particle forces in the packing, which is related to the scaling function of the contact peak by $\mathcal{F}(\lambda)=\int_0^\infty df\, f P(f) e^{-\lambda f}$ (refs 18,40,57), thus also decays as a power law $P(f)\sim f^{\theta}$ at small forces. Note that, as observed in ref. 58, this phenomenon is closely related to what happens to the distribution of frozen fields in the SK model[59], which is thought to explain the Coulomb gap in interacting electron systems[47]. Beyond the contact peak, the slower decay of pair correlation function follows another power-law $g(r)\sim(r-1)^{-\alpha}$ that describes the abundance of quasi-contacts. These scalings of $g(r)$ are crucial for determining the mechanical stability of packings[48,58]. Perturbing a packing breaks some contacts with small forces, while also forming new contacts from what previously were quasi-contacts. On the basis of this observation, a scaling relation for mechanical stability $\alpha=1/(2+\theta)$ can be

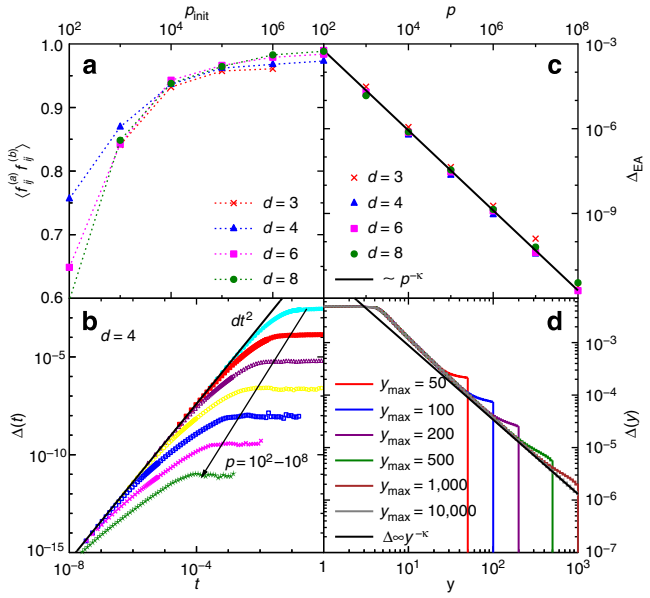

Figure 3 | Force network and position overlaps in the fractal basin. (**a**) Overlap between the force network edges $f_{ij}=0,1$ that connect two particles i and j in two glass configurations a and b (at pressure $p_{\rm f}=10^{10}$), obtained by independent compression of the same initial configuration at initial pressure $p_{\rm init}$ (Supplementary Note 2). (**b**) Time-evolution of the mean-square displacement $\Delta(t)$ for glasses at $p=10^2$, 10^3, 10^4, 10^5, 10^6, 10^7 and 10^8 in $d=4$. The solid line indicates the ballistic dt^2 behaviour. The long-time value is the cage size $d\Delta_{\rm EA}$. (**c**) The pressure evolution of the cage size $\Delta_{\rm EA}$ in various dimension closely follows a power-law $\sim p^{-\kappa}$ with the theoretical value $\kappa=1.41575$. (**d**) Analytical results for the order parameter $\Delta(y)$ at $2^{\rm d}\varphi/d=10$. Increasing the cutoff $y_{\rm max}\sim p$ indicates that the scaling regime $\Delta(y)\sim y^{-\kappa}$ extends to all y. (Supplementary Note 1)

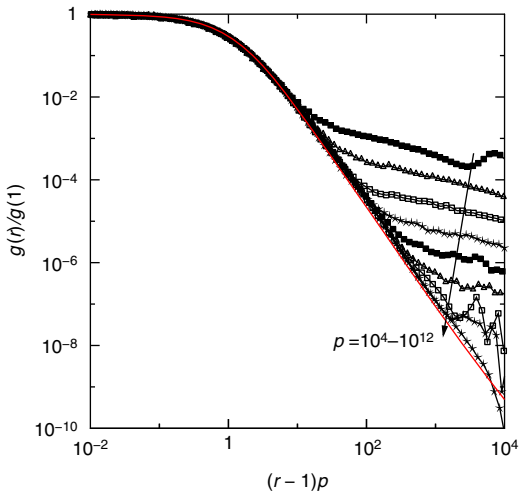

Figure 4 | Pair correlation function close to jamming. Scaling of the contact peak of the pair correlation $g(r)$. The theory predicts that in the limit $p\to\infty$ one has $g(r)/g(1)=\mathcal{F}(\lambda)$ with $\lambda=(r-1)p$. Points are numerical data for $g(r)$ in $d=4$ obtained at several pressures $p=10^4$, $10^5,\ldots,10^{12}$; the full line is the theoretical prediction.

derived[58]. Remarkably, the exponents predicted by our theory, $\alpha = 0.41269$ and $\theta = 0.42311$, satisfy this scaling relation to within numerical precision. Previous estimates of these exponents were also obtained by numerical simulation. The quasi-contact exponent α has been measured by several groups in dimension d ranging from 2 to 13, all obtaining roughly $\alpha \approx 0.4$ (refs 39,40,48,57,60), the most precise estimates being $\alpha = 0.41(3)$ (ref. 40). The weak force exponent θ is, however, more difficult to measure, and values spanning the interval $\theta \approx 0.2 \div 0.45$ have been reported[40,48]. Although the existence of a second exponent $\theta' < \theta$ has been shown to affect the tail of $P(f)$ (ref. 48), its role in determining $\mathcal{F}(\lambda)$ and its large-dimensional scaling remains to be clarified. Additional numerical simulations are thus needed to test the theory more stringently.

A prediction for the force distribution $P(f)$ at jamming is also available from the theory. However, because this function is not completely determined by the scaling regime, it must be obtained by solving the full equations that describe the marginal phase. Numerically, the function $\mathcal{F}(\lambda) = \int_0^\infty df f P(f) e^{-\lambda f}$ is much easier to measure than $P(f)$ because it only depends on structural information, while, in hard spheres, forces must be determined from the collision dynamics. The theoretical prediction for the scaling function $\mathcal{F}(\lambda)$ is tested against numerical simulations in Fig. 4, with very good agreement.

Discussion

We have described the marginal phase that is present below the Gardner transition for hard spheres in $d = \infty$. Using this result we have shown that the jamming transition happens inside the marginal phase and that its low-dimensional criticality is well described by our approach. This analysis opens the way for analytically determining many other properties of jammed packings, such as their shear modulus[61], and the properties of avalanches[62].

The microscopic explanation of several hitherto mysterious properties of low-temperature glasses might also emerge from this work. (i) A well-attested observation is that glasses that are quenched deeply and rapidly continue to age after the quench, even if the system is well inside the glass phase and there is no activation energy or volume that allows for changes of basin[5]. If the same final pressure is reached with a slower annealing protocol, the subsequent ageing effect is less marked. This observation becomes quite natural if we think in terms of the diagram of Fig. 2. Metastable states that may be reached with a faster annealing become fractal (that is, undergo a Gardner transition) at pressures much closer to the liquid–glass transition, while the better annealed ones reached with slower protocols only do so at higher pressures. (ii) A related observation is that the existence of a transition from stable to marginal glass along the threshold line (marked by a diamond in Fig. 2) might affect the ageing dynamics after a deep and very fast quench[9,46], inducing a change in the ageing properties as a function of the final temperature akin to those observed in some polymer glasses[63]. A more detailed investigation of these effects will require characterizing the off-equilibrium dynamics in the marginal phase[9,46], which at present is only poorly understood. (iii) Another fact that does not fit the standard picture is the observation of dynamical heterogeneities in low-temperature glasses[64,65] at timescales much shorter than the inter-basin relaxation. Low-temperature dynamical heterogeneities with a diverging four-point susceptibility are a signature of a fractal phase[30], while they are expected to be absent within a simple glass basin. Here the theory is well developed, but a detailed comparison with experiments is still missing. (iv) The quantum properties of low-temperature glasses has long been described in terms of a set of tunnelling two-level systems (TLS), characterized by a non-trivial distribution of barriers[66]. The origin of TLS is not understood, but it has been proposed, using schematic models, that TLS might be due to low-energy excitations associated with a marginally stable phase of the kind discussed above[67]. Within our approach, an exact computation of the quantum properties at very low temperatures is viable, and one may hence expect that two-level systems could be put on a first-principle footing. (v) As mentioned in the introduction, Johari-Goldstein processes can be interpreted as transitions between sub-basins belonging to a same metabasin[4,5,26]. This interpretation naturally explains their many-body origin[68], but transforming this physical intuition in a theoretically solid explanation requires additional work. Although in the limit $d \to \infty$ the equilibrium supercooled liquid region is always far away from the marginal phase, where Johari-Goldstein-like relaxations are expected, we suspect that activated processes, which are absent in $d \to \infty$ but play a prominent role in $d = 3$, might bring supercooled liquids much closer to the marginal region. The contribution of Johari-Goldstein processes to glass dynamics may thus be enhanced in $d = 3$ compared with the mean-field prediction. In the $d = \infty$ limit, the barriers controlling inter-basin relaxation should indeed scale as d, and the largest ones, separating sub-basins, as $d^{1/3}$, which suggest the existence of quasi-localized excitations[69] (stringlike, in three dimensions[70]).

Methods

Analytical results. Results are based on the combination of analytical and numerical methods. Analytical results come from the exact solution of hard spheres in the limit $d \to \infty$, which, for convenience, is obtained using the replica method, but any other method would give the same result. The fractal phase is described by a function $\Delta(y)$ for $y \in [1, y_{\max}]$, as in the SK model[29]. The cutoff $y_{\max} \sim p$ diverges with pressure. With these definitions, $\Delta_{EA} = \Delta(y_{\max})$ is the mean square displacement in the smallest sub-basins, where $\Delta(y)$ can be computed by numerically solving a set of coupled integro-differential equations obtained from the replica approach (Supplementary Note 1).

Numerical simulations. Numerical results are obtained by standard event-driven molecular dynamic simulations in $d = 3$–8 (refs 39,40). Slow compressions are made using the Lubachevsky-Stillinger algorithm[39] (Supplementary Note 2).

References

1. Goldstein, M. Viscous liquids and the glass transition: a potential energy barrier picture. *J. Chem. Phys.* **51,** 3728–3739 (1969).
2. Debenedetti, P. G. & Stillinger, F. H. Supercooled liquids and the glass transition. *Nature* **410,** 259–267 (2001).
3. Cavagna, A. Supercooled liquids for pedestrians. *Phys. Rep.* **476,** 51–124 (2009).
4. Goldstein, M. Communications: comparison of activation barriers for the Johari-Goldstein and alpha relaxations and its implications. *J. Chem. Phys.* **132,** 041104 (2010).
5. Hachenberg, J. *et al.* Merging of the α and β relaxations and aging via the Johari-Goldstein modes in rapidly quenched metallic glasses. *Appl. Phys. Lett.* **92,** 131911 (2008).
6. de Souza, V. K. & Wales, D. J. Energy landscapes for diffusion: Analysis of cage-breaking processes. *J. Chem. Phys.* **129,** 164507 (2008).
7. Heuer, A. Exploring the potential energy landscape of glass-forming systems: from inherent structures via metabasins to macroscopic transport. *J. Phys. Condens. Matter* **20,** 373101 (2008).
8. Yardimci, H. & Leheny, R. L. Aging of the Johari-Goldstein relaxation in the glass-forming liquids sorbitol and xylitol. *J. Chem. Phys.* **124,** 214503 (2006).
9. Cugliandolo, L. F. & Kurchan, J. On the out-of-equilibrium relaxation of the Sherrington-Kirkpatrick model. *J. Phys. A* **27,** 5749–5772 (1994).
10. Bernal, J. D., Mason, J. & Knight, K. R. Radial distribution of the random close packing of equal spheres. *Nature* **194,** 957–958 (1962).
11. Pusey, P. N. & van Megen, W. Phase behaviour of concentrated suspensions of nearly hard colloidal spheres. *Nature* **320,** 340–342 (1986).
12. van Megen, W., Underwood, S. M. & Pusey, P. N. Nonergodicity parameters of colloidal glasses. *Phys. Rev. Lett.* **67,** 1586–1589 (1991).
13. Brambilla, G. *et al.* Probing the equilibrium dynamics of colloidal hard spheres above the mode-coupling glass transition. *Phys. Rev. Lett.* **102,** 085703 (2009).
14. Lechenault, F., Dauchot, O., Biroli, G. & Bouchaud, J.-P. Critical scaling and heterogeneous superdiffusion across the jamming/rigidity transition of a granular glass. *Europhys. Lett.* **83,** 46003 (2008).

15. Krzakala, F. & Kurchan, J. Landscape analysis of constraint satisfaction problems. *Phys. Rev. E* **76,** 021122 (2007).
16. Mézard, M. & Parisi, G. Glasses and replicas. in *Structural Glasses and Supercooled Liquids: Theory, Experiment and Applications* (eds Wolynes, P. G. & Lubchenko, V.) (Wiley & Sons, 2012).
17. Götze, W. *Complex Dynamics of Glass-Forming Liquids: A Mode-Coupling Theory* Vol. 143 (Oxford University Press, 2009).
18. Parisi, G. & Zamponi, F. Mean-field theory of hard sphere glasses and jamming. *Rev. Mod. Phys.* **82,** 789–845 (2010).
19. O'Hern, C. S., Langer, S. A., Liu, A. J. & Nagel, S. R. Random packings of frictionless particles. *Phys. Rev. Lett.* **88,** 075507 (2002).
20. van Hecke, M. Jamming of soft particles: geometry, mechanics, scaling and isostaticity. *J. Phys. Condens. Matter* **22,** 033101 (2010).
21. Liu, A. J., Nagel, S. R., van Saarloos, W. & Wyart, M. The jamming scenario - an introduction and outlook. in *Dynamical Heterogeneities and Glasses* (eds Berthier, L., Biroli, G., Bouchaud, J.-P., Cipelletti, L. & van Saarloos, W.) (Oxford University Press, 2011).
22. Ikeda, A., Berthier, L. & Sollich, P. Unified study of glass and jamming rheology in soft particle systems. *Phys. Rev. Lett.* **109,** 018301 (2012).
23. Wyart, M., Silbert, L. E., Nagel, S. R. & Witten, T. A. Effects of compression on the vibrational modes of marginally jammed solids. *Phys. Rev. E* **72,** 051306 (2005).
24. Brito, C. & Wyart, M. Heterogeneous dynamics, marginal stability and soft modes in hard sphere glasses. *J. Stat. Mech. Theor. Exp.* **2007,** L08003 (2007).
25. Brito, C. & Wyart, M. Geometric interpretation of previtrification in hard sphere liquids. *J. Chem. Phys.* **131,** 024504 (2009).
26. Kirkpatrick, T. R. & Wolynes, P. G. Stable and metastable states in mean-field Potts and structural glasses. *Phys. Rev. B* **36,** 8552–8564 (1987).
27. Kirkpatrick, T. R. & Thirumalai, D. Dynamics of the structural glass transition and the p-spin-interaction spin-glass model. *Phys. Rev. Lett.* **58,** 2091–2094 (1987).
28. Wolynes, P. & Lubchenko, V (eds). *Structural Glasses and Supercooled Liquids: Theory, Experiment, and Applications* (Wiley, 2012).
29. Parisi, G. Order parameter for spin-glasses. *Phys. Rev. Lett.* **50,** 1946–1948 (1983).
30. Mezard, M., Parisi, G. & Virasoro, M. A. *Spin Glass Theory and Beyond* (World Scientific, Singapore, 1987).
31. Cugliandolo, L. F. & Kurchan, J. Analytical solution of the off-equilibrium dynamics of a long-range spin-glass model. *Phys. Rev. Lett.* **71,** 173–176 (1993).
32. Bouchaud, J.-P., Cugliandolo, L. F., Kurchan, J. & Mézard, M. Out of equilibrium dynamics in spin-glasses and other glassy systems. in *Spin Glasses and Random Fields* (ed. Young, A. P.) (World Scientific, 1998).
33. Gardner, E. Spin glasses with p-spin interactions. *Nucl. Phys. B* **257,** 747–765 (1985).
34. Kirkpatrick, T. R. & Wolynes, P. G. Connections between some kinetic and equilibrium theories of the glass transition. *Phys. Rev. A* **35,** 3072–3080 (1987).
35. Kurchan, J., Parisi, G. & Zamponi, F. Exact theory of dense amorphous hard spheres in high dimension. I. The free energy. *J. Stat. Mech. Theor. Exp.* **2012,** P10012 (2012).
36. Kurchan, J., Parisi, G., Urbani, P. & Zamponi, F. Exact theory of dense amorphous hard spheres in high dimension. II. The high density regime and the Gardner transition. *J. Phys. Chem. B* **117,** 12979–12994 (2013).
37. Witten, E. Quarks, atoms, and the 1/n expansion. *Phys. Today* **33,** 38–43 (1980).
38. Georges, A. & Yedidia, J. S. How to expand around mean-field theory using high-temperature expansions. *J. Phys. A* **24,** 2173–2192 (1991).
39. Skoge, M., Donev, A., Stillinger, F. H. & Torquato, S. Packing hyperspheres in high-dimensional Euclidean spaces. *Phys. Rev. E* **74,** 041127 (2006).
40. Charbonneau, P., Corwin, E. I., Parisi, G. & Zamponi, F. Universal microstructure and mechanical stability of jammed packings. *Phys. Rev. Lett.* **109,** 205501 (2012).
41. Goodrich, C. P., Liu, A. J. & Nagel, S. R. Finite-size scaling at the jamming transition. *Phys. Rev. Lett.* **109,** 095704 (2012).
42. Tarjus, G. An overview of the theories of the glass transition. in *Dynamical Heterogeneities and Glasses* (eds Berthier, L., Biroli, G., Bouchaud, J.-P., Cipelletti, L. & van Saarloos, W.) (Oxford University Press, 2011).
43. Berthier, L. & Biroli, G. Theoretical perspective on the glass transition and amorphous materials. *Rev. Mod. Phys.* **83,** 587–645 (2011).
44. Montanari, A. & Ricci-Tersenghi, F. On the nature of the low-temperature phase in discontinuous mean-field spin glasses. *Eur. Phys. J. B* **33,** 339–346 (2003).
45. Montanari, A. & Ricci-Tersenghi, F. Cooling-schedule dependence of the dynamics of mean-field glasses. *Phys. Rev. B* **70,** 134406 (2004).
46. Rizzo, T. Replica-symmetry-breaking transitions and off-equilibrium dynamics. *Phys. Rev. E* **88,** 032135 (2013).
47. Müller, M. & Pankov, S. Mean-field theory for the three-dimensional Coulomb glass. *Phys. Rev. B* **75,** 144201 (2007).
48. Lerner, E., During, G. & Wyart, M. Low-energy non-linear excitations in sphere packings. *Soft Matter* **9,** 8252–8263 (2013).
49. Krzakala, F. & Zdeborova, L. Following Gibbs states adiabatically: the energy landscape of mean-field glassy systems. *Europhys. Lett.* **90,** 66002 (2010).
50. De Dominicis, C. & Kondor, I. Eigenvalues of the stability matrix for Parisi solution of the long-range spin-glass. *Phys. Rev. B* **27,** 606–608 (1983).
51. Charbonneau, P., Ikeda, A., Parisi, G. & Zamponi, F. Glass transition and random close packing above three dimensions. *Phys. Rev. Lett.* **107,** 185702 (2011).
52. Moukarzel, C. F. Isostatic phase transition and instability in stiff granular materials. *Phys. Rev. Lett.* **81,** 1634–1637 (1998).
53. Tkachenko, A. V. & Witten, T. A. Stress propagation through frictionless granular material. *Phy. Rev. E* **60,** 687–696 (1999).
54. Roux, J.-N. Geometric origin of mechanical properties of granular materials. *Phys. Rev. E* **61,** 6802–6836 (2000).
55. Pankov, S. Low-temperature solution of the Sherrington-Kirkpatrick model. *Phys. Rev. Lett.* **96,** 197204 (2006).
56. Ikeda, A., Berthier, L. & Biroli, G. Dynamic criticality at the jamming transition. *J. Chem. Phys.* **138,** 12A507–17AA (2013).
57. Donev, A., Torquato, S. & Stillinger, F. H. Pair correlation function characteristics of nearly jammed disordered and ordered hard-sphere packings. *Phys. Rev. E* **71,** 011105 (2005).
58. Wyart, M. Marginal stability constrains force and pair distributions at random close packing. *Phys. Rev. Lett.* **109,** 125502 (2012).
59. Sommers, H.-J. & Dupont, W. Distribution of frozen fields in the mean-field theory of spin glasses. *J. Phys. C* **17,** 5785–5793 (1984).
60. Atkinson, S., Stillinger, F. H. & Torquato, S. Detailed characterization of rattlers in exactly isostatic, strictly jammed sphere packings. *Phys. Rev. E* **88,** 062208 (2013).
61. Yoshino, H. Replica theory of the rigidity of structural glasses. *J. Chem. Phys.* **136,** 214108–214136 (2012).
62. Le Doussal, P., Müller, M. & Wiese, K. J. Avalanches in mean-field models and the Barkhausen noise in spin-glasses. *Europhys. Lett.* **91,** 57004 (2010).
63. Struik, L. C. E. Physical aging in plastics and other glassy materials. *Polymer Eng. Sci.* **17,** 165–173 (1977).
64. Vollmayr-Lee, K., Kob, W., Binder, J.-L. & Zippelius, A. Dynamical heterogeneities below the glass transition. *J. Chem. Phys.* **116,** 5158–5166 (2002).
65. Ballesta, P., Duri, A. & Cipelletti, L. Unexpected drop of dynamical heterogeneities in colloidal suspensions approaching the jamming transition. *Nat. Phys.* **4,** 550–554 (2008).
66. Anderson, P. W., Halperin, B. I. & Varma, C. M. Anomalous low-temperature thermal properties of glasses and spin glasses. *Philos. Mag.* **25,** 1–9 (1972).
67. Kuhn, R. Universality in glassy low-temperature physics. *Europhys. Lett.* **62,** 313 (2003).
68. Capaccioli, S., Paluch, M., Prevosto, D., Wang, L.-M. & Ngai, K. L. Many-body nature of relaxation processes in glass-forming systems. *J. Phys. Chem. Lett.* **3,** 735–743 (2012).
69. Xu, N., Vitelli, V., Liu, A. J. & Nagel, S. R. Anharmonic and quasi-localized vibrations in jammed solids modes for mechanical failure. *Europhys. Lett.* **90,** 56001 (2010).
70. Stevenson, J. D. & Wolynes., P. G. A universal origin for secondary relaxations in supercooled liquids and structural glasses. *Nat. Phys.* **6,** 62–68 (2010).

Acknowledgements

We thank Silvio Franz for an extremely useful discussion, and Daphne Klotsa for help with Figure 1. We also thank Ludovic Berthier, Carolina Brito, Florent Krzakala, Edan Lerner, Federico Ricci-Tersenghi, Tommaso Rizzo, Hajime Yoshino and Matthieu Wyart for many interesting exchanges related to this work. Financial support was provided by the European Research Council through ERC grant agreement no. 247328 and ERC grant NPRGGLASS. P.C. acknowledges support from the Alfred P. Sloan Foundation and from National Science Foundation Grant no. NSF DMR-1055586.

Author contributions

P.C., J.K., G.P., P.U. and F.Z. designed the research, performed the research and wrote the paper.

Additional information

Supplementary Information accompanies this paper at http://www.nature.com/naturecommunications

Competing financial interests: The authors declare no competing financial interests.

Reprints and permission information is available online at http://npg.nature.com/reprintsandpermissions/

How to cite this article: Charbonneau, P. *et al.* Fractal free energy landscapes in structural glasses. *Nat. Commun.* 5:3725 doi: 10.1038/ncomms4725 (2014).

SUPPLEMENTARY NOTE 1
EXACT SOLUTION OF HARD SPHERES IN THE LIMIT OF INFINITE DIMENSIONS

This supplementary note reviews the exact solution of a hard-sphere system in high dimensions, which is obtained through the replica method in the full replica symmetry breaking (fullRSB) scheme [1]. We sketch here the main logical steps that allow one to obtain the results presented in this work. A detailed derivation will be presented elsewhere.

General formulation

Within the general RFOT framework, the disordered glass states of a particle system are assumed to be metastable and long-lived. Their lifetime is indeed assumed to diverge in the mean-field $d \to \infty$ limit, where d is the spatial dimension. These glass states therefore need to be described through appropriate extensions of standard statistical mechanics, which in practice consists of using the replica method, density functional (or Thouless-Anderson-Palmer) methods, or dynamical methods (see Ref. [2] for a complete review). Although all of these approaches are conceptually equivalent, in this paper we use the replica method, which is technically the simplest by far. The reader might be confused by the fact that the replica method is usually introduced to average over quenched disorder [3], which is absent from the interaction potential of standard glass formers. As it has long been recognized [4, 5], the main technical problem in these systems is that the emergence of metastable glassy states is not associated with a clear pattern of symmetry breaking, hence an individual glass state cannot be selected through a properly defined symmetry breaking field. This problem can, however, be surmounted by introducing a random external field, which is sent to zero at the end of the computation. The presence of this external field breaks translational symmetry and selects one among the many possible glass states. Replicas are therefore needed to properly take into account the presence of this external random field [4, 5]. This idea has been turned into a concrete computational scheme that exploits the tools from standard liquid theory [6]. Although a full description of this construction is beyond the scope of the current work, some of us have recently written detailed reviews that the reader may find useful [7, 8].

The infinite dimensional limit

We now focus on a system of identical d-dimensional particles, interacting through the hard-sphere potential $v(x)$. Temperature is irrelevant for this system and can be set to one, without loss of generality. The starting point is the virial expansion for the entropy $\mathcal{S}$ as a function of the density field of hard-sphere particles. Taking the high-dimensional limit allows us to retain only the first two terms of the virial series, as Frisch and Percus have shown [9]. Hence the entropy of the system is a functional of the density profile $\rho(x)$ (that expresses the density of particles at point x) given by

$$\mathcal{S}[\rho(x)] = \int \mathrm{d}^d x\, \rho(x)[1 - \log \rho(x)] + \frac{1}{2} \int \mathrm{d}^d x \mathrm{d}^d y \rho(x)\rho(y) f(x-y), \tag{1}$$

where $f(x) = e^{-v(x)} - 1 = -\theta(D - |x|)$ is the Mayer function and D is the diameter of the hard spheres. The first term in this expression is the ideal gas contribution, while the second term is the second virial correction and represents the mean-field density-density interaction. The equilibrium entropy of the system is obtained by maximizing the entropy, i.e., by solving the stationarity equation $\delta\mathcal{S}/\delta\rho(x) = 0$. At low density, the system is in a homogeneous liquid phase and the solution is $\rho(x) = \rho$. As density increases the system undergoes a first-order phase transition to a crystalline phase, whose symmetry is only known in low dimensions. If crystallization is avoided, the system instead enters a metastable supersaturated liquid phase [10]. In three dimensions, particular care must be taken both in numerical simulations and in experiments to avoid the crystal phase [8], but in $d > 3$, crystal nucleation is dynamically suppressed [11, 12], enabling the study and characterization of amorphous states.

As discussed above, a well-established theoretical approach to study these amorphous states consists of coupling the system to a spatial external random field that destabilizes the crystal and favors glassy configurations [4, 5]. One is then left with the problem of studying m copies (or replicas) of the original system infinitesimally weakly coupled together. In other words, each particle in the original problem now becomes a "molecule" made by m identical "atoms", each atom being a copy of the original particle. This molecular liquid can be studied with the standard tools of liquid theory [6, 7]. In high dimensions, the Frisch-Percus argument [9] that we discussed above for the non-replicated system also applies to the replicated one [8]. The entropy of the replicated system (or molecular liquid)

then reads

$$\mathcal{S}[\rho(\overline{x})] = \int \mathrm{d}\overline{x}\, \rho(\overline{x})[1 - \log \rho(\overline{x})] + \frac{1}{2}\int \mathrm{d}\overline{x}\mathrm{d}\overline{y}\rho(\overline{x})\rho(\overline{y})f(\overline{x}-\overline{y}), \tag{2}$$

where $\rho(\overline{x})$ is the single molecule density field [7, 8] and is a function of m d-dimensional coordinates $\overline{x} = \{x_1 \dots x_m\}$ that describe the configuration of a single molecule. Again the two terms represent the ideal gas term and the mean-field density-density interaction, and the density field is determined by maximizing the entropy, i.e., by solving the stationarity equations $\delta\mathcal{S}/\delta\rho(\overline{x}) = 0$. The phase diagram can be obtained by changing the parameter m after analytically continuing the expression to non integer values, following the approach described in Refs. [5–8].

A crucial remark is that the molecular liquid remains translationally and rotationally invariant, because the random external field is eliminated through the introduction of replicas. Requiring that the density profile be translationally and rotationally invariant leaves us with a function $\rho(\overline{x})$ that can only depend on the scalar products $q_{ab} = u_a \cdot u_b$, where $x_a = X + u_a$ with $X = m^{-1}\sum_a x_a$ being the center of mass of all x_a. A detailed study of this problem provides two important results [13]: *(i)* the analytical expression for the replicated entropy in Eq. (2) in terms of the matrix $\hat{q}$ of the scalar products of the displacement vectors u_a in the infinite dimension limit, *(ii)* the proof that the exact solution of the stationarity equation gives the same replicated entropy as that computed within a Gaussian approximation for $\rho(\overline{x})$.

Let us write down the replicated entropy that was obtained this way in Refs. [13, 14]. We also define the Gaussian ansatz for the density field

$$\rho(\overline{u}) = \frac{\rho m^{-d}}{(2\pi)^{(m-1)d/2}\det(\hat{A}^{(m,m)})^{d/2}} \exp\left[-\frac{1}{2}\sum_{a,b}^{1,m-1}\left(\hat{A}^{m,m}\right)^{-1}_{ab} u_a \cdot u_b\right], \tag{3}$$

where $\langle \hat{q} \rangle = d\hat{A}$. Note that because of translational invariance, $\sum_a u_a = 0$, hence $\sum_a q_{ab} = 0$ and $\sum_a A_{ab} = 0$. Hence, the matrix $\hat{A}$ is not invertible and thus $\rho(\overline{u})$ only depends on $\hat{A}^{m,m}$, which is the matrix obtained from $\hat{A}$ by eliminating the last column and and the last row. The replicated entropy in terms of a rescaled matrix $\hat{\alpha} = \frac{d^2}{D^2}\hat{A}$ is given in Eq. (45) of Ref. [13] as

$$s[\hat{\alpha}] = \frac{\mathcal{S}[\hat{\alpha}]}{N} = 1 - \log\rho + d\log m + \frac{(m-1)d}{2}\log(2\pi e D^2/d^2) + \frac{d}{2}\log\det(\hat{\alpha}^{m,m}) - \frac{d}{2}\widehat{\varphi}\,\mathcal{F}\left(2\hat{\alpha}\right) \ , \tag{4}$$

where s is the replicated entropy per particle. We have also introduced a reduced packing fraction $\widehat{\varphi} = 2^d\varphi/d$ that remains finite at the glass transition, even when $d \to \infty$. The function $\mathcal{F}(\hat{v})$ is defined as follows

$$\mathcal{F}(\hat{v}) = \lim_{n\to 0} \sum_{n_1,\dots,n_m:\sum_a n_a = n} \frac{n!}{n_1!\dots n_m!} \exp\left[-\frac{1}{2}\sum_{a=1}^{m} v_{aa}\frac{n_a}{n} + \frac{1}{2}\sum_{a,b}^{m} v_{ab}\frac{n_a n_b}{n^2}\right] . \tag{5}$$

The above expression for the entropy must be maximized with respect to the matrix $\hat{\alpha}$ and one can therefore study the stationarity equations $\delta s[\hat{\alpha}]/\delta\hat{\alpha} = 0$. By constraining the form of $\hat{\alpha}$ one can restrict the parameter space over which to search for a solution. The simplest ansatz assumes that $\hat{\alpha}$ is completely symmetric under replica exchange, i.e., $\alpha_{ab} = \frac{1}{2}\Delta(\delta_{ab} - 1/m)$, and thus only depends on a single parameter Δ. It can be shown [5, 7, 8] that this structure corresponds to the standard 1-step replica symmetry breaking (1RSB) computation for models with quenched disorder, which is precisely the structure assumed in the original RFOT scenario [15, 16]. The hard-sphere phase diagram obtained this way was reported in Ref. [8]. Starting from Eq. (4), however, Ref. [14] showed that this 1RSB solution is unstable in some regions of the pressure-density phase diagram.

FullRSB equations

In the present paper we discuss the results obtained by assuming a fullRSB structure for the matrix $\hat{\alpha}$ that solves the stationarity equations. A review of the fullRSB construction is given in Ref. [3]. FullRSB matrices form a closed algebra and can be parametrized by a function over the interval $[0, 1]$, as we discuss below. By analogy with spin glass models, the fullRSB structure is expected to provide the exact solution of the model when the 1RSB solution is unstable. The correctness of the fullRSB solution can be proven by studying its (marginal) stability. We have obtained indications of marginal stability (by studying the relevant eigenvalue and found that it is identically zero in the fullRSB phase), but we leave a full discussion, i.e., a computation of all eigenvalues, for future work.

In order to illustrate the fullRSB construction we introduce the fundamental object of our theoretical approach, that is, the matrix of mean-square displacements between atoms in a molecule defined by

$$\Delta_{ab} = \frac{d}{D^2}\langle (u_a - u_b)^2 \rangle = \alpha_{aa} + \alpha_{bb} - 2\alpha_{ab} \, . \tag{6}$$

This matrix is analogous to the overlap matrix of the replica solution of mean-field spin glasses [3]. Not only does it encode the order parameter of the system, but its structure also reflects how the free energy minima are organized [1, 3, 17]. The 1RSB ansatz consists of taking a replica symmetric matrix $\Delta_{ab} = \Delta$ for $a \neq b$, which corresponds to the replica symmetric form of $\hat{\alpha}$ discussed above. The connection with dynamics is as follows. Consider a particle trajectory $x_i(t)$ and define the mean-square displacement

$$\Delta(t) = \frac{1}{N}\sum_{i=1}^{N} |x_i(t) - x_i(0)|^2 \, . \tag{7}$$

At the 1RSB level we then have

$$\lim_{t\to\infty} \Delta(t) = \Delta, \tag{8}$$

where $t \to \infty$ means that we take the limit of the mean-square displacement for times that are large compared to the microscopic timescale but no larger than the lifetime of the metastable state in which the dynamics is trapped.

The fullRSB solution can be constructed as a sequence of kRSB solutions in the limit where k diverges. The first step is a 2RSB solution. In this case we divide the values that can be assumed by the replica indexes a and b into m/m_1 groups each of them containing m_1 possible values. We pose that $\Delta_{ab} = \Delta_2$ if both a and b are in the same group and $\Delta_{ab} = \Delta_1$ otherwise. The 2RSB entropy can be obtained by plugging this ansatz in Eq. (4) and optimizing the result over Δ_1 and Δ_2. In order to go beyond the 2RSB ansatz we can construct a 3RSB matrix by dividing each of the m/m_1 blocks into m_1/m_2 blocks each containing m_2 values and by saying that $\Delta_{ab} = \Delta_3$ if we are in the same sub block. Iterating this procedure constructs a kRSB solution. In the fullRSB limit, where $k \to \infty$, the matrix Δ_{ab} can be parametrized by a continuous function $\Delta(x)$ over the interval $x \in [m, 1]$. Roughly speaking, the "index" x (corresponding to the continuum limit of the m_1 indices) selects a given hierarchical level, associated to the hierarchical structure of the subbasins sketched in Fig. 1. The replicated entropy, which can then be written as a function of $\Delta(x)$, is given by

$$\mathcal{S}_{\text{fullRSB}} = -m\int_m^1 \frac{\mathrm{d}x}{x^2}\log\left[\frac{x\Delta(x)}{m} + \int_x^1 \mathrm{d}z\frac{\Delta(z)}{m}\right] - \widehat{\varphi}\, e^{-\Delta(m)/2}\int_{-\infty}^{\infty}\mathrm{d}h\, e^h[1 - e^{mf(m,h)}] \, , \tag{9}$$

where the function f satisfies the equation

$$\frac{\partial f(x,h)}{\partial x} = \frac{1}{2}\dot{\Delta}(x)\left[\frac{\partial^2 f(x,h)}{\partial h^2} + x\left(\frac{\partial f(x,h)}{\partial h}\right)^2\right] \, , \tag{10}$$

with initial condition $f(1,h) = \log\left(\frac{1}{2} + \frac{1}{2}\mathrm{erf}\left[\frac{h}{\sqrt{2\Delta(1)}}\right]\right)$. Note that Eq. (10) was first obtained by one of us in the solution of the Sherrington-Kirkpatrick model [1, 3] and is the key connection between hard spheres and spin glasses.

The expressions above give the replicated entropy within a fullRSB ansatz as a function of $\Delta(x)$. To obtain thermodynamic results, we must, however, optimize the function over $\Delta(x)$. To write (and solve numerically) the stationarity equations, it is convenient to introduce in Eqs. (9) and (10) a rescaled variable $y = x/m$ and a rescaled function $\widehat{f}(y,h) = mf(x,h) = -\frac{h^2\theta(-h)}{2\gamma(y)} + \widehat{j}(y,h)$, and to introduce Lagrange multipliers $\widehat{P}(y,h)$ and $\widehat{P}(1/m,h)$ that enforce both the Parisi equation (Eq. (10)) and its initial condition. The final variational equations for the fullRSB

solution are

$$
\begin{aligned}
\Delta(y) &= \frac{\gamma(y)}{y} - \int_y^{1/m} \frac{dz}{z^2}\gamma(z) \ , \qquad \Leftrightarrow \qquad \gamma(y) = y\Delta(y) + \int_y^{1/m} \mathrm{d}z \Delta(z) \ , \\
\widehat{j}(1/m,h) &= m \log\left[\frac{1}{2}\left(1+\mathrm{erf}\left(\frac{h}{\sqrt{2m\gamma(1/m)}}\right)\right)\right] + \frac{h^2\theta(-h)}{2\gamma(1/m)} \ , \\
\frac{\partial \widehat{j}(y,h)}{\partial y} &= \frac{1}{2}\frac{\dot{\gamma}(y)}{y}\left[-\frac{\theta(-h)}{\gamma(y)} + \frac{\partial^2 \widehat{j}(y,h)}{\partial h^2} - 2y\frac{h\theta(-h)}{\gamma(y)}\frac{\partial \widehat{j}(y,h)}{\partial h} + y\left(\frac{\partial \widehat{j}(y,h)}{\partial h}\right)^2\right] \ , \\
\widehat{P}(1,h) &= e^{-\Delta(1)/2 - \frac{h^2\theta(-h)}{2\gamma(1)} + \widehat{j}(1,h)} \ , \\
\frac{\partial \widehat{P}(y,h)}{\partial y} &= -\frac{1}{2}\frac{\dot{\gamma}(y)}{y} e^{-h}\left\{\frac{\partial^2[e^h \widehat{P}(y,h)]}{\partial h^2} - 2y\frac{\partial}{\partial h}\left[e^h \widehat{P}(y,h)\left(-\frac{h\theta(-h)}{\gamma(y)} + \frac{\partial \widehat{j}(y,h)}{\partial h}\right)\right]\right\} \ , \\
\kappa(y) &= \frac{\widehat{\varphi}}{2}\int_{-\infty}^{\infty} \mathrm{d}h\, e^h\, \widehat{P}(y,h)\left(-\frac{h\theta(-h)}{\gamma(y)} + \widehat{j}'(y,h)\right)^2 \ , \\
\frac{1}{\gamma(y)} &= y\kappa(y) - \int_1^y dz \kappa(z) \ .
\end{aligned}
\tag{11}
$$

Here dots denote derivatives with respect to y and primes denote derivatives with respect to h. These equations can be solved numerically either by discretizing them on a grid, or by going to their corresponding finite kRSB iterative representation, that is

$$
\begin{aligned}
\widehat{\Delta}_i &= \frac{\widehat{\gamma}_i}{y_i} + \sum_{j=i+1}^{k}\left(\frac{1}{y_j} - \frac{1}{y_{j-1}}\right)\widehat{\gamma}_j \ , \\
\widehat{j}(1/m,h) &= m \log \Theta\left(\frac{h}{\sqrt{2m\widehat{\gamma}_k}}\right) + \frac{h^2\theta(-h)}{2\widehat{\gamma}_k} \ , \\
\widehat{j}(y_i,h) &= \frac{1}{y_i}\log\left[\int_{-\infty}^{\infty} dz\, K_{\widehat{\gamma}_i,\widehat{\gamma}_{i+1},y_i}(h,z)\, e^{y_i \widehat{j}(y_{i+1},z)}\right] \ , \qquad i = 1 \cdots k-1 \ , \\
\widehat{P}(y_1,h) &= e^{-\widehat{\Delta}_1/2 - \frac{h^2\theta(-h)}{2\widehat{\gamma}_1} + \widehat{j}(y_1,h)} \ , \\
\widehat{P}(y_i,h) &= \int dz\, K_{\widehat{\gamma}_{i-1},\widehat{\gamma}_i,y_{i-1}}(z,h)\, \widehat{P}(y_{i-1},z)\, e^{z-h}\, e^{-y_{i-1}\widehat{j}(y_{i-1},z) + y_{i-1}\widehat{j}(y_i,h)} \qquad i = 2, \cdots, k \ , \\
\widehat{\kappa}_i &= \frac{\widehat{\varphi}}{2}\int_{-\infty}^{\infty} \mathrm{d}h\, e^h\, \widehat{P}(y_i,h)\left(-\frac{h\theta(-h)}{\widehat{\gamma}_i} + \widehat{j}'(y_i,h)\right)^2 \ , \\
\frac{1}{\widehat{\gamma}_i} &= y_{i-1}\widehat{\kappa}_i - \sum_{j=1}^{i-1}(y_j - y_{j-1})\widehat{\kappa}_j \ ,
\end{aligned}
\tag{12}
$$

where

$$
K_{\widehat{\gamma},\widehat{\gamma}',y}(h,z) = \frac{\exp\left[-\frac{y}{2}\left(\frac{(z-h)^2}{\widehat{\gamma}-\widehat{\gamma}'} - \frac{h^2\theta(-h)}{\widehat{\gamma}} + \frac{z^2\theta(-z)}{\widehat{\gamma}'}\right)\right]}{\sqrt{2\pi(\widehat{\gamma}-\widehat{\gamma}')/y}} \ . \tag{13}
$$

When k is sufficiently large, the results of the discrete kRSB equations should converge to the continuum fullRSB ones, which is the numerical strategy we employ here.

Numerical solution of the fullRSB equations, and the emergence of a scaling regime at large pressure

The fullRSB equations are formulated in terms of a function $\Delta(y)$ for $y = x/m \in [1, 1/m]$. It can be shown that the pressure associated with a given glass basin is $p \propto 1/m$ [8, 14], and therefore taking the limit $m \to 0$ corresponds to bringing the system to the jamming limit $p \to \infty$. In this limit the variable y extends over the range $[1, \infty)$.

To gain insights into the behavior of the fullRSB solution in the jamming limit, we numerically solve Eqs. (12). To simplify the numerical analysis, we fix $m = 0$ in the equation, while keeping a finite cutoff $y < y_{\max} \equiv 1/m$, as is obviously needed for numerical purposes. We indeed expect that the most important role of m, when $m \to 0$, is to fix the cutoff scale, the other contributions being but small perturbations in that limit. The results of this numerical computation are given in Fig. 3 of the main text. We observe two important effects. First, repeating the procedure for several values of k (recall that k is the number of RSB steps) reveals that the result does not depend on k when k is large. We find $k = 100$ to be a good choice and can be taken as representative of the fullRSB limit $k = \infty$. Second, when $y_{\max} = 1/m \to 0$, the solution converges to a limit curve and we observe that $\Delta(y) \sim y^{-1-c}$ when $y \to \infty$, with c close (but not equal) to 0.5. Note that from Eq. (11) one has $\dot{\gamma}(y) = y\dot{\Delta}(y)$ and therefore $\gamma(y \to \infty) \sim y^{-c}$.

The second observation is crucial for the subsequent analysis. Based on the results of the numerical solution of Eq. (12), we can look for an asymptotic scaling solution of the fullRSB equations (11) when $m = 0$ and $y \to \infty$ that has the form

$$\Delta(y) \sim \Delta_\infty y^{-1-c} \,, \tag{14}$$

$$\gamma(y) \sim \gamma_\infty y^{-c} \,, \tag{15}$$

$$\widehat{j}(y,h) \sim -\frac{c}{2y} J(hy^b/\sqrt{\gamma_\infty}) \,, \tag{16}$$

$$\widehat{P}(y,h) \sim \begin{cases} y^c p_0(hy^c) & \text{for } h \sim -y^{-c} \,, \\ y^a p_1(hy^b) & \text{for } |h| \sim y^{-b} \,, \\ p_2(h) & \text{for } h \gg y^{-b} \,. \end{cases} \tag{17}$$

In the following, we define rescaled variables $z = hy^c$ and $t = hy^b/\sqrt{\gamma_\infty}$.

A comment on this scaling form is in order. The result for $\Delta(y)$ and $\gamma(y)$ has been motivated above. The form of $\widehat{j}(y,h)$ can be guessed by first considering its asymptotic limits $h \to \pm\infty$, where, using Eq. (11) with Eq. (15), we can show that $\widehat{j}(y, h \to -\infty) \sim -c/(2y)$ and that $\widehat{j}(y, h \to \infty) = 0$. Then Eq. (16) is a natural guess, with a function $J(t)$ that goes from $J(t \to \infty) = 0$ to $J(t \to -\infty) = 1$ and varies on a scale y^b, that remains to be determined.

Motivating Eq. (17) is a bit harder and goes in three logical steps. First, the existence of three different scaling regimes is clearly visible in the numerical solution of Eq. (12). Second, the analysis of the continuum equation for $\widehat{P}(y,h)$, under the assumption given in Eq. (15), allows one to prove the scalings associated to p_0 and p_2 in Eq. (17). This part of the analysis is technically involved and will be reported elsewhere. Third, the existence of a matching regime associated with p_1 is needed for consistency. The fact that exponent b is the same as the one for $\widehat{j}(y,h)$ is a natural and simple choice that, as we will show, is consistent with the equations. The p_0 and p_1 regimes are matched by requiring that $p_0(z) \sim |z|^\theta$ for small z, and $p_1(z \to -\infty) \sim |z|^\theta$, with $\theta = \frac{c-a}{b-c}$ in such a way that the two power laws are matched. Similarly, matching the p_1 and p_2 regimes requires that $p_1(z \to \infty) \sim z^{-\alpha}$ with $\alpha = a/b$, and $p_2(h) \sim h^{-\alpha}$ for $h \to 0$. We therefore obtain information on the asymptotic behavior of the functions p_0, p_1, p_2.

Analytical calculation of the exponents at jamming

The exponents a, b, and c can be now determined by inserting the scaling form given by Eqs. (14)-(17) in the fullRSB equations (11) in the limit $m \to 0$.

Pluging Eq. (15) and Eq. (16) into the equation for $\widehat{j}$ and taking the $y \to \infty$ limit, gives that a non trivial equation for the scaling function J exists if and only if $b = (1+c)/2$ and is given by

$$\frac{c}{2} J''(t) = -tJ'(t)\left(\frac{1+c}{2} - c\theta(-t)\right) + J(t) - \theta(-t) + \frac{c^2}{4} J'(t)^2 \,, \tag{18}$$

with the boundary conditions $J(-\infty) = 1$ and $J(\infty) = 0$. This equation admits a unique solution once the value of c has been fixed. This treatment thus provides a relation between b and c as well as an equation for $J(t)$.

We can now turn to the scaling of $\widehat{P}$, focusing on the matching regime in Eq. (17), where $\widehat{P}(y,h) \sim y^a p_1(hy^b)$. Plugging this asymptotic form in the equation for $\widehat{P}(y,h)$ given in Eq. (11) and taking the $y \to \infty$ limit, we find once again that a non trivial result only exists for $b = (1+c)/2$. We can also write down an equation for the scaling function $p_1(t)$ that is given by

$$\frac{c}{2} p_1''(t) = (a - c\theta(-t)) p_1(t) + \left(\frac{1+c}{2} - c\theta(-t)\right) t p_1'(t) - \frac{c^2}{2}\left[p_1'(t)J'(t) + p_1(t)J''(t)\right] \,. \tag{19}$$

This equation is linear in p_1 and can be seen as an eigenvalue problem for a. We need to find the eigenfunction p_1 that behaves like $|t|^\theta$ when $t \to -\infty$ and like $t^{-\alpha}$ when $t \to \infty$, and is such that $p_1(t) > 0$. This eigenvalue problem admits a unique solution for a that depends on c through c itself and through $J(t)$. In this way at fixed c we can compute the other two exponents a and b, and the functions $J(t)$ and $p_1(t)$.

We last need to fix the value of c. A general consequence of the fullRSB equations is the following relation

$$1 = \frac{\widehat{\varphi}}{2} \int_{-\infty}^{\infty} \mathrm{d}h e^h \widehat{P}(y,h) \widetilde{f}''(y,h)^2 \qquad \widetilde{f}(y,h) = -\frac{h^2\theta(-h)}{2} + \gamma(y)\widehat{j}(y,h) \ , \tag{20}$$

which can be derived directly from Eq. (11) and is nothing but the mathematical statement of marginal stability of the fullRSB solution. By deriving this equation with respect to y, by using the fullRSB equations, and by plugging in the result for the scaling ansatz in the limit $y \to \infty$, we obtain the following relation

$$\frac{1}{2} = \frac{\int_{-\infty}^{\infty} dt\, p_1(t) \left[\theta(-t) + \frac{c}{2} J''(t)\right]^2 \left[\theta(t) - \frac{c}{2} J''(t)\right]}{\int_{-\infty}^{\infty} dt\, p_1(t) \left[\frac{d}{dt}\left(\theta(-t) + \frac{c}{2} J''(t)\right)\right]^2} \ . \tag{21}$$

Because the right hand side is a function of c, this condition indeed fixes the value of c.

The equations above can be solved numerically with arbitrary precision to obtain the exponents a, b , and c and

$$\kappa = 1 + c \ , \qquad \alpha = a/b \ , \qquad \theta = \frac{c-a}{b-c} \ . \tag{22}$$

The results are

$$\begin{aligned} a &= 0.29213\ldots \ , & b &= 0.70787\ldots \ , & c &= 0.41574\ldots \ , \\ \alpha &= 0.41269\ldots \ , & \theta &= 0.42311\ldots \ , & \kappa &= 1.41574\ldots \ , \end{aligned} \tag{23}$$

where the precision is given by the last digit and depends on the cutoff used to discretize the asymptotic equations given in Eqs. (18), (19), and (23).

Pair correlation function and the Coulomb gap

We now show that the three critical exponents α, θ, and κ are connected to measurable quantities.

First, recall that $\Delta(y) \sim y^{-1-c} \sim y^{-\kappa}$ when y is large. Within the fullRSB solution, the value of $\Delta(y)$ associated with the largest y is the so-called Edwards-Anderson order parameter $\Delta_{\mathrm{EA}} = \Delta(y_{\max})$, which can be connected to the long-time limit of the mean-square displacement (7) in the glass by $\lim_{t\to\infty} \Delta(t) = \Delta_{\mathrm{EA}}$. In other words, Δ_{EA} is the Debye-Waller factor. Recalling that $y_{\max} = 1/m \propto p$, we conclude that $\Delta_{\mathrm{EA}} \propto p^{-\kappa}$, i.e., that the Debye-Waller factor of the glass vanishes with pressure with the anomalous exponent κ, contrary to what happens in a hard-sphere crystal where $\Delta_{\mathrm{EA}} \propto p^{-2}$.

Second, it is possible to show that the function $\widehat{P}(y,h)$ is connected to the pair correlation function of the glass, but the derivation is fairly long, thus details will be given elsewhere. For now, we note that the pair correlation function $g(r)$ is given, for $r = D(1 + h/d)$ and $d \to \infty$, by

$$g(h) = \theta(h) \int_{-\infty}^{\infty} dz\, e^{z-h}\, \gamma_{\Delta(1/m)}(h-z)\, \widehat{P}(1/m, z)\, e^{-m f(1/m,z)} \ , \tag{24}$$

where $\gamma_\Delta(x)$ is a centered and normalized Gaussian of width Δ. From this relation, one can show that the exponent α controls the power-law divergence of the pair correlation function upon approaching contact through the relation $g(h) \sim h^{-\alpha}$, as was numerically observed in several studies [18].

One can also show that $g(h)$ develops a delta peak for $h \propto 1/p$ upon approaching jamming. The integral of this peak gives that the number of contacts is equal to $2d$. Jammed packings are thus *predicted* to be isostatic. Note that Eq. (20), i.e., marginal stability, plays a crucial role in the derivation of isostaticity. Upon approaching jamming, the contact peak is described by a scaling function [8], which is basically the Laplace transform of $p_0(z)$. Hence the exponent θ enters in the scaling of the delta peak, and is connected to the probability distribution of inter-particle forces $P(f)$ [8, 19]. In this way one can show that for small f, $P(f) \sim f^\theta$.

The three exponents, α, θ , and κ are therefore connected to the scaling of measurable quantities by $\Delta_{\mathrm{EA}}(p \to \infty) \sim p^{-\kappa}$, $g(h \to 0) \sim h^{-\alpha}$, $P(f \to 0) \sim f^\theta$, and are related to the exponents a, b, and c that enter in Eq. (17) by the three relations (22). Note that within numerical error we find that $a + b = 1$ (see Eq. (23)) even if at the moment we are not capable of deriving this relation analytically. Coupling the relation $a + b = 1$ with all the other scaling relations implies that $\alpha = 1/(2 + \theta)$, a scaling relation that was first derived in Ref. [20].

Fractal structure of the basins

The function $\Delta(y)$ can also be used to look directly at the structure of hierarchically organized states [3]. In the 1RSB picture of the glass transition, at the dynamical or mode-coupling transition point the liquid minimum of the free energy landscape breaks down into an exponential number of minima organized according to their free energy (here, internal entropy). From this landscape one can study the number of metastable states having internal entropy s

$$\mathcal{N}(s) = \mathrm{e}^{N\Sigma(s)}, \tag{25}$$

where N is the size of the system. In the fullRSB picture the state structure is organized in a hierarchical way. Suppose that we are able to sample configurations from a given state a. We then introduce the mean-square distance between two of these configurations, labeled a and b, as $\Delta_{ab} = \frac{1}{N}\sum_{i=1}^{N} |x_i^{(a)} - x_i^{(b)}|^2$. To be more concrete, let us "lump" all of the states that are at a mutual distance that is less then Δ within a metabasin in which the total internal entropy is s. We can then try to determine how many of them there are, $\mathcal{N}(s,\Delta)$. In this way we obtain a coarse-grained description of the configurational entropy on the scale Δ defined by

$$\mathcal{N}(s,\Delta) = \mathrm{e}^{N\Sigma(s,\Delta)}\,. \tag{26}$$

From this definition it follows that $\Sigma(s,\Delta(1)) = \Sigma_{\mathrm{L}}(s)$, where $\Sigma_{\mathrm{L}}(s)$ is the configurational entropy of the largest metabasin. The connection between $\Sigma(s,\Delta)$ and the mean-square displacement profile $\Delta(y)$ can be obtained as follows. We first highlight the dependence on m of the profile $\Delta(y;m)$, and we introduce the inverse function $y(\Delta;m)$. The standard 1RSB expression that relates the configurational entropy of metabasins having internal entropy s to Δ is then given by

$$my(\Delta(1;m);m) = m = \frac{\partial\Sigma(s,\Delta(1;m))}{\partial s} = \frac{\partial\Sigma_{\mathrm{L}}(s)}{\partial s}\,, \tag{27}$$

where we have used the fact that $y(\Delta(1;m);m) = 1$. This relation holds for the most coarse-grained version of the configurational entropy. If we reduce the coarse graining on states we have on a fixed scale Δ, then we obtain

$$my(\Delta,m) = \frac{\partial\Sigma(s,\Delta)}{\partial s}\,. \tag{28}$$

Equation (27) relates m to the total internal entropy s of the metabasins we are looking for, on a fixed scale of metabasin width Δ.

It can be shown that at equilibrium the metabasins entropies on a scale Δ are *independent random variables* distributed according to $\mathcal{P}_\Delta(s) \propto e^{my(\Delta;m)s}$ [3, 17] , and therefore the typical value of s on a scale Δ is $s_{\mathrm{typ}}(\Delta) \propto 1/y(\Delta)$. From this result it follows that close to jamming, there is a large region of (small) Δ, where $y(\Delta) \sim \Delta^{1/\kappa}$. In this region, when increasing Δ from the smallest Δ_{EA} to the larger values, one finds that the total basin size grows as $s_{\mathrm{typ}}(\Delta) \sim 1/y(\Delta) \sim \Delta^{1/\kappa} \sim \sqrt{\Delta}^{2/\kappa}$ (recalling that Δ is the squared distance between configurations). Hence the basins in phase space form a fractal with dimension $2/\kappa = 1.41267\cdots$.

Out-of-equilibrium dynamics

Following a quench from high temperature or, in the case of hard spheres, from low pressure, at initial time $t = 0$, a macroscopic system relaxes without reaching equilibrium. During this process, the two-time correlation function

$$\Delta(t,t_w) = \frac{1}{N}\sum_{i=1}^{N} |x_i(t) - x_i(t_w)|^2 \tag{29}$$

never becomes a function of $(t - t_w)$, where t_w is the waiting time after the quench. Instead, relaxation becomes progressively slower as t_w becomes larger, i.e., as the system *ages*. Rather surprisingly, one may infer from a static calculation some features of the out-of-equilibrium dynamics. This result follows from two different facts:
(i) The constant pressure dynamics relaxes up to a density at which the free energy landscape disconnects into separate basins. This *threshold* level [21] is also the one at which the basins lose their stability and become marginal.
(ii) At long times, the almost-stable states visited by the dynamics are sampled with equal probability. This property emerges in the mean-field out-of-equilibrium solution [21, 22], of which there is no clear general explanation yet.
If we compute the function $\Delta(y)$ with the value of m fixed not by maximizing the free energy (minimizing the entropy)

as in the equilibrium computation, but rather by demanding that for $m = m_{\rm th}$ the stability of the solution be marginal (the replicon associated with the largest value of Δ in the Parisi ansatz vanishes), it may be shown that properties *i)* and *ii)* imply that the values of pressure, free energy, and other thermodynamic properties coincide with the asymptotic properties obtained from the dynamics. The fluctuation-dissipation ratio is then given by $m_{\rm th}y(\Delta; m_{\rm th})$, when the time-dependent mean-square displacement is $\Delta(t, t_w) = \Delta$ [22].

SUPPLEMENTARY NOTE 2
MOLECULAR DYNAMICS SIMULATIONS

Molecular dynamics simulations of N=8000 identical hard spheres in d=3, 4, 6, and 8 evolving in a cubic box under periodic boundary conditions are performed using a modified version of the event-driven code described in Refs. [11, 18]. Hard spheres of unit diameter D and unit mass m naturally express time t in units of $\sqrt{\beta m D^2}$ at fixed unit inverse temperature β. Glasses are obtained from compressing very low-density fluids using a Lubachevski-Stillinger algorithm with, in $d > 3$, a slow particle growth rate of $\dot{\gamma} = 3\times10^{-4}$ [11]. Slow compaction of the fluid makes it fall out of equilibrium near the dynamical transition and evolves the resulting glass arbitrarily close to jamming, approximating an adiabatic state following [18]. In d=3, a rapid initial growth with $\dot{\gamma} = 3 \times 10^{-2}$, in order to prevent crystal formation [18], is followed by the slower growth rate once the system is well within the glass, i.e., $p \gtrsim 10^3$.

Using these glass configurations as starting point for fixed-density simulations, the mean-square displacement $\Delta(t) = \frac{1}{N}\sum_i \langle |x_i(t) - x_i(0)|^2 \rangle$ is obtained (Fig. 3(b) from the main text). Rattlers, which are identified by compressing each glass up to $p = 10^{10}$ [18] and identifying particles with fewer than $d+1$ force contacts, i.e., with pair distances that are smaller than $D + 100/p$, are removed from the averaging. The long-time plateau then gives $\lim_{t\to\infty} \Delta(t)/d = \Delta_{\rm EA}$, where the Debye-Waller factor $\Delta_{\rm EA}$ estimates the average cage size in the glass.

In order to capture the state structure upon approaching jamming, we track the evolution of the overlap of the underlying force network $\langle f_{ij}^{(a)} f_{ij}^{(b)} \rangle$ for glasses at different pressures. The force network is obtained by performing pairwise comparisons between 100 configurations (a and b) that evolve from a glass initially obtained as described above. This configuration then undergoes a molecular dynamics simulation sufficiently long for the initial positions to decorrelate, but while staying within the same glass state, i.e., for their mean-square displacement to reach the plateau height of the Debye-Waller factor. Each of the configurations is then independently compressed to $p = 10^{10}$ at $\dot{\gamma} = 3 \times 10^{-4}$. At that pressure a very large fraction of the force network is already defined. Then if particles i and j are within a distance $D + 100/p$ from each other they are considered to be part of the force network and hence $f_{ij} = 1$; for all other pairs of particles $f_{ij} = 0$. Rattlers in configurations a and b are removed from the analysis. Note that the results from Fig. 3(a) are qualitatively insensitive to the choice of cutoff as long as it is near the crossover between weak contacts and quasi-contacts [18].

SUPPLEMENTARY REFERENCES

[1] Giorgio Parisi, "Order parameter for spin-glasses," Physical Review Letters **50**, 1946–1948 (1983).

[2] Tommaso Castellani and Andrea Cavagna, "Spin glass theory for pedestrians," Journal of Statistical Mechanics: Theory and Experiment **2005**, P05012 (2005).

[3] M. Mézard, G. Parisi, and M. A. Virasoro, *Spin glass theory and beyond* (World Scientific, Singapore, 1987).

[4] T. R. Kirkpatrick and D. Thirumalai, "Comparison between dynamical theories and metastable states in regular and glassy mean-field spin models with underlying first-order-like phase transitions," Phys. Rev. A **37**, 4439–4448 (1988).

[5] Rémi Monasson, "Structural glass transition and the entropy of the metastable states," Phys. Rev. Lett. **75**, 2847–2850 (1995).

[6] M. Mézard and G. Parisi, "A tentative replica study of the glass transition," Journal of Physics A: Mathematical and General **29**, 6515–6524 (1996).

[7] M. Mezard and G. Parisi, "Glasses and replicas," in *Structural Glasses and Supercooled Liquids: Theory, Experiment and Applications*, edited by P.G.Wolynes and V.Lubchenko (Wiley & Sons, 2012).

[8] Giorgio Parisi and Francesco Zamponi, "Mean-field theory of hard sphere glasses and jamming," Rev. Mod. Phys. **82**, 789–845 (2010).

[9] H. L. Frisch and J. K. Percus, "High dimensionality as an organizing device for classical fluids," Phys. Rev. E **60**, 2942–2948 (1999).

[10] A. Cavagna, "Supercooled liquids for pedestrians," Physics Reports **476**, 51–124 (2009).

[11] Monica Skoge, Aleksandar Donev, Frank H. Stillinger, and Salvatore Torquato, "Packing hyperspheres in high-dimensional Euclidean spaces," Phys. Rev. E **74**, 041127 (2006).

[12] Patrick Charbonneau, Atsushi Ikeda, Giorgio Parisi, and Francesco Zamponi, "Glass transition and random close packing above three dimensions," Phys. Rev. Lett. **107**, 185702 (2011).

[13] J. Kurchan, G. Parisi, and F. Zamponi, "Exact theory of dense amorphous hard spheres in high dimension. I. the free energy," Journal of Statistical Mechanics: Theory and Experiment **2012**, P10012 (2012).
[14] Jorge Kurchan, Giorgio Parisi, Pierfrancesco Urbani, and Francesco Zamponi, "Exact theory of dense amorphous hard spheres in high dimension. II. The high density regime and the gardner transition," J. Phys. Chem. B **117**, 12979–12994 (2013).
[15] T. R. Kirkpatrick and P. G. Wolynes, "Stable and metastable states in mean-field Potts and structural glasses," Phys. Rev. B **36**, 8552–8564 (1987).
[16] T. R. Kirkpatrick and D. Thirumalai, "Dynamics of the structural glass transition and the p-spin-interaction spin-glass model," Phys. Rev. Lett. **58**, 2091–2094 (1987).
[17] M Mézard, G Parisi, N Sourlas, G Toulouse, and M Virasoro, "Nature of the spin-glass phase," Physical Review Letters **52**, 1156–1159 (1984).
[18] Patrick Charbonneau, Eric I. Corwin, Giorgio Parisi, and Francesco Zamponi, "Universal microstructure and mechanical stability of jammed packings," Phys. Rev. Lett. **109**, 205501 (2012).
[19] Aleksandar Donev, Salvatore Torquato, and Frank H. Stillinger, "Pair correlation function characteristics of nearly jammed disordered and ordered hard-sphere packings," Physical Review E **71**, 011105 (2005).
[20] Matthieu Wyart, "Marginal stability constrains force and pair distributions at random close packing," Phys. Rev. Lett. **109**, 125502 (2012).
[21] L. F. Cugliandolo and J. Kurchan, "Analytical solution of the off-equilibrium dynamics of a long-range spin-glass model," Phys. Rev. Lett. **71**, 173–176 (1993).
[22] L. F. Cugliandolo and J. Kurchan, "On the out-of-equilibrium relaxation of the Sherrington–Kirkpatrick model," Journal of Physics A: Mathematical and General **27**, 5749–5772 (1994).